



# Inhibition of the Hypoxia-Inducible Factor 1 $\alpha$ -Induced Cardiospecific HERNA1 Enhance-Templated RNA Protects From Heart Disease

**BACKGROUND:** Enhancers are genomic regulatory elements conferring spatiotemporal and signal-dependent control of gene expression. Recent evidence suggests that enhancers can generate noncoding enhancer RNAs, but their (patho)biological functions remain largely elusive.

**METHODS:** We performed chromatin immunoprecipitation-coupled sequencing of histone marks combined with RNA sequencing of left ventricular biopsies from experimental and genetic mouse models of human cardiac hypertrophy to identify transcripts revealing enhancer localization, conservation with the human genome, and hypoxia-inducible factor 1 $\alpha$  dependence. The most promising candidate, hypoxia-inducible enhancer RNA (*HERNA1*), was further examined by investigating its capacity to modulate neighboring coding gene expression by binding to their gene promoters by using chromatin isolation by RNA purification and  $\Delta$ N-BoxB tethering-based reporter assays. The role of *HERNA1* and its neighboring genes for pathological stress-induced growth and contractile dysfunction, and the therapeutic potential of *HERNA1* inhibition was studied in gapmer-mediated loss-of-function studies in vitro using human induced pluripotent stem cell-derived cardiomyocytes and various in vivo models of human pathological cardiac hypertrophy.

**RESULTS:** *HERNA1* is robustly induced on pathological stress. Production of *HERNA1* is initiated by direct hypoxia-inducible factor 1 $\alpha$  binding to a hypoxia-response element in the histoneH3-lysine27acetylation marks-enriched promoter of the enhancer and confers hypoxia responsiveness to nearby genes including synaptotagmin XVII, a member of the family of membrane-trafficking and Ca<sup>2+</sup>-sensing proteins and *SMG1*, encoding a phosphatidylinositol 3-kinase-related kinase. Consequently, a substrate of *SMG1*, ATP-dependent RNA helicase upframeshift 1, is hyperphosphorylated in a *HERNA1*- and *SMG1*-dependent manner. In vitro and in vivo inactivation of *SMG1* and *SYT17* revealed overlapping and distinct roles in modulating cardiac hypertrophy. Finally, in vivo administration of antisense oligonucleotides targeting *HERNA1* protected mice from stress-induced pathological hypertrophy. The inhibition of *HERNA1* postdisease development reversed left ventricular growth and dysfunction, resulting in increased overall survival.

**CONCLUSIONS:** *HERNA1* is a novel heart-specific noncoding RNA with key regulatory functions in modulating the growth, metabolic, and contractile gene program in disease, and reveals a molecular target amenable to therapeutic exploitation.

Peter Mirtschink, MD\*  
Corinne Bischof, PhD\*  
Minh-Duc Pham, MSc  
Rahul Sharma, PhD  
Sanjay Khadayate, PhD  
Geetha Rossi, MSc  
Niklaus Fankhauser, PhD  
Shuyang Traub MD, PhD  
Samuel Sossalla, MD, PhD  
Eman Hagag, MSc  
Corinne Berthonneche, PhD  
Alexandre Sarre, PhD  
Sebastian. N. Stehr, MD  
Phillip Grote, PhD  
Thierry Pedrazzini, PhD  
Stefanie Dimmeler, PhD  
Wilhelm Krek, PhD  
Jaya Krishnan, PhD

\*Drs Mirtschink and Bischof contributed equally.

**Key Words:** heart failure ■ hypoxia ■ RNA

Sources of Funding, see page 2791

© 2019 The Authors. *Circulation* is published on behalf of the American Heart Association, Inc., by Wolters Kluwer Health, Inc. This is an open access article under the terms of the [Creative Commons Attribution Non-Commercial-NoDerivs License](#), which permits use, distribution, and reproduction in any medium, provided that the original work is properly cited, the use is noncommercial, and no modifications or adaptations are made.

<https://www.ahajournals.org/journal/circ>

## Clinical Perspective

### What Is New?

- Chromatin immunoprecipitation–coupled sequencing of histone marks combined with RNA sequencing of ventricular biopsies from various mouse models of human cardiac hypertrophy were performed to identify hypoxia-inducible factor 1 $\alpha$ –dependent transcripts from enhancer regions, showing conservation with the human genome.
- In following in vivo and in vitro screening approaches, *HERNA1* was identified as robustly upregulated in cardiac ventricles on pressure overload, featuring characteristics of an intergenic enhancer RNA.
- *HERNA1* binding to the promoter region of the neighboring genes *Syt17* and *Smg1* triggers a hypoxia-responsive transcriptional response leading to pathological growth, a glycolytic phenotype and a *Syt17*-driven contractile dysfunction corresponding to pressure-overload heart disease.

### What Are the Clinical Implications?

- Suppression of stress-induced *Herna1* production in mice resolved established cardiomyopathy through repression of *Syt17* and *Smg1* transcription, indicating that a tight coupling of enhancer transcription and successive induction of promoters in their vicinity is disease relevant.
- Data obtained from left ventricular biopsies of patients experiencing pressure overload–induced heart failure recapitulate the expression profile of translational mouse models and, hence, indicate a potential disease-driving role for the HERNA1-SMG1-SYT17 axis in humans as well.
- The beneficial effects of *HERNA1* depletion in induced pluripotent stem cell–human cardiomyocytes protecting from structural, metabolic, and functional remodeling suggests *HERNA1* as a novel RNA target for the treatment of heart failure.

Chronic heart failure is characterized by clinical symptoms of cardiac dysfunction and represents the culmination of prolonged left ventricular growth in response to pathological stressors including ischemia, hypertension, aortic stenosis, and genetic mutations. Despite being the leading cause of hospitalization and mortality worldwide, therapeutic strategies remain limited.<sup>1</sup> Of particular concern is the fact that current treatment modalities have limited potential to treat the underlying cause of heart disease. Hence, targeting key causative drivers of disease development and progression have the potential to lead to more personalized and effective therapies.

Recent developments in transcriptomics and epigenetics has led to a deeper understanding of the mech-

anistic basis of gene regulation and revealed novel species of noncoding RNA.<sup>2</sup> Of these, enhancer-templated RNAs (eRNAs) represent a novel class of gene-modulating noncoding RNAs that are templated at genomic enhancers.<sup>3,4</sup> Enhancers are regulatory DNA elements that bind transcription factors to induce gene transcription through the formation of secondary structures that mediate the interaction of the enhancer with the promoter.<sup>5</sup> Enhancers are activated in a cell-type and context-dependent manner that arises from the range of transcription factors that are active in specific cell types or on a particular stimulus.<sup>6</sup> Transcription at enhancer elements positively correlates with enhancer activity,<sup>3</sup> and is characterized by high histone 3 lysine 4 monomethylation (H3K4me1) and low H3K4 trimethylation (me3).<sup>7,8</sup> In addition to H3K4 methylation, enrichment of H3K27 acetylation and absence of the repressive H3K27me3 signature also serve as indicators of transcriptional activity at enhancer regions.<sup>9</sup> eRNA transcription has been described to induce transcription of either one or both neighboring coding 5' and 3' genes.<sup>10,11</sup> Recent studies have identified eRNAs that are differentially expressed and correlate with the expression of nearby coding genes in mouse models of cardiomyopathy, and human patients experiencing heart disease in comparison with healthy subjects.<sup>2,12</sup> Thus, the specific modulation of cell type and stress-responsive eRNAs has the potential to very precisely influence pathophysiologic gene networks.

Hypoxia-inducible factors (HIFs) are heterodimeric transcription factors composed of HIF $\alpha$  and HIF $\beta$  subunits that occupy central roles in oxygen homeostasis<sup>13</sup> and the pathogenesis of human disease including cancer and cardiovascular disease.<sup>14</sup> They are activated in hypoxic tissue to induce a transcriptional program embracing coding and noncoding RNA transcripts that are entrusted to modulate both the supply and consumption of oxygen. However, it is unclear if HIFs also activate transcription of eRNAs to afford cell and signal specificity of select HIF output responses. In the present study, we identify *hypoxia-inducible factor 1 $\alpha$ -activated eRNA (HERNA1)*, as critical determinant in pressure-overload heart disease and demonstrate how in vivo antisense oligonucleotides (ASO)-mediated inactivation of *HERNA1* prevents stress-induced cardiac pathogenesis and dramatically improves overall survival in diseased mice.

## METHODS

The data and analytic methods will be made available to other researchers. Some study material can be made available on request. Methods are expanded in the [online-only Data Supplement](#).

## Study Approval

Left ventricular samples were obtained from subjects with hypertrophic cardiomyopathy, aortic stenosis, or dilated

cardiomyopathy and from healthy subjects. Institutional review board approval was obtained and subjects provided informed consent. Maintenance and animal experimentation were in accordance with institutional and Swiss Federal Veterinary Office guidelines.

## Statistics

Statistical analyses of dependent samples were performed by paired *t* test (Excel), of unpaired samples, by unpaired (multiple) *t* tests, and, if not normally distributed, by Mann–Whitney *U* test (Prism 5.0). For multiple group comparisons, 1- or 2-way ANOVA analyses followed by a Dunnett or Tukey multiple comparison posttest were used as indicated in the respective figure legends. If measurements were taken on the same experimental units, repeated-measures ANOVA was used. *P* values of <0.05 were considered as significant. Unless otherwise indicated, *n* indicates the number of individual experiments.

## RESULTS

### HERNA1 Identification and Correlation With Pathology

To identify potential HIF-regulated eRNAs, we performed genome-wide epigenetic and transcriptomic analysis of cardiac left ventricular biopsies of 2 distinct mouse models of cardiac hypertrophy: surgery-induced aortic stenosis (transaortic constriction [TAC]) and ventricular-specific deletion of the *von Hippel Lindau* (*Vhl*) gene (referred to as *Vhl cKO*).<sup>15,16</sup> *Vhl* protein is a negative regulator of oxygen-sensitive Hif $\alpha$  subunits and its deletion leads to constitutive activation of Hif1 $\alpha$  and spontaneous cardiac hypertrophy.<sup>16,17</sup> Chromatin immunoprecipitation–coupled sequencing was performed on biopsies of these models to identify enhancer domains as marked by monomethylated histone H3 lysine 4 (H3K4me1) signals, and regions of active or poised transcription as indicated by trimethylated histone H3 lysine 4 (H3K4me3) marks.<sup>18</sup> RNA sequencing was also performed to detect differentially expressed transcripts. We cross-referenced our data against ENCODE and other published data sets<sup>11,19,20</sup> to select for RNAs with enhancer localization, human genomic conservation, and HIF1 $\alpha$  dependence (described in [Figures I and IIA through IIC in the online-only Data Supplement](#)). This analysis unveiled *HERNA1*, featuring characteristics of an intergenic enhancer RNA specifically upregulated in diseased cardiac ventricles with considerable sequence conservation among mammalian species (Figure 1A and 1B and [Figure IIIA and IIIB in the online-only Data Supplement](#)). Chromatin immunoprecipitation–coupled sequencing of left ventricular biopsies of mice subjected to TAC or 1 kidney 1-clip (1K1C) or *Vhl cKO* mice revealed a concordant increase in H3K4me3 signal at the *Herna1* locus (Figure 1A and 1C), a finding consistent with elevated H3K4ac27 marks observed by

targeted chromatin immunoprecipitation in neonatal mouse cardiomyocytes (NMCs) subjected to hypoxia and in mouse disease models including TAC, *Vhl cKO*, and 1K1C (Figure 1D). It is intriguing that these analyses also revealed parallel changes in mRNA and protein expression of neighboring genes *Smg1* and *Syt17* and partial positional conservation of this cluster structure in various species (Figure 1B, 1E through 1H and [Figure IIIA and IIIB in the online-only Data Supplement](#)). *Herna1* induction occurred concomitant to elevated *Smg1* and *Syt17* expression in mouse surgical and genetic models of cardiomyopathy and in primary cardiomyocytes exposed to hypoxia, and demonstrated Hif1 $\alpha$  sensitivity (Figure 1E through 1H and [Figure IVA and IVB in the online-only Data Supplement](#)).

### HERNA1 Is a HIF1 $\alpha$ -Dependent Noncoding RNA With Enhancer Function

Because *Herna1* transcription correlated with Hif1 $\alpha$  activation, we investigated if *Herna1* is a direct target of Hif1 $\alpha$ . In silico analysis of the *HERNA1* promoter revealed a conserved hypoxia response element (HRE) at position –121 bp and –195 bp upstream of the transcription start site in the mouse and human genome, respectively (Figure 2A). To assess Hif1 $\alpha$  binding at this HRE, we performed Hif1 $\alpha$  chromatin immunoprecipitation from nuclear extracts of NMCs subjected to normoxia (20% O<sub>2</sub>) or hypoxia (3% O<sub>2</sub>). Hif1 $\alpha$  associated at the HRE of the *HERNA1* promoter in native chromatin specifically in NMCs subjected to hypoxia (Figure 2B). Moreover, mutation of the conserved *HERNA1* HRE resulted in blunted *HERNA1* promoter-luciferase reporter activity on ectopic expression of HIF1 $\alpha$  lacking the oxygen-dependent degradation domain (HIF1 $\alpha$  $\Delta$ ODD) or stimulation with phenylephrine (PE; Figure 2C). HIF1 $\alpha$  binding at the *Herna1* promoter and HIF1 $\alpha$ -dependent promoter activation were confirmed in left ventricular biopsies of *Hif1 $\alpha$  fl/fl* and *Hif1 $\alpha$  cko* mice and in *Vhl fl/fl* and *Vhl fl/fl cko* mice, respectively, in isolated NMCs of these lines ([Figure IVC through IVH in the online-only Data Supplement](#)). Conserved HREs were not detected in promoters of *Smg1* or *Syt17*, and luciferase reporter assays with their respective promoters failed to demonstrate hypoxia or Hif1 $\alpha$  sensitivity ([Figure IVI and IVJ in the online-only Data Supplement](#)). To assess enhancer function of *HERNA1*, we cloned a 2.9-kb fragment containing *HERNA1* and additional flanking sequences including the HRE, downstream of the SV-40 promoter driving luciferase expression,<sup>9</sup> and quantified luciferase activity in response to HIF1 $\alpha$  $\Delta$ ODD expression (Figure 2D). Reporter assays revealed a Hif1 $\alpha$  dose-dependent increase in enhancer activity of the luciferase promoter reporter, whereas negligible effects on luciferase activity were observed with a 3-kb control genomic fragment encompassing the *peroxisome proliferator activated receptor  $\gamma$*  (*Ppar $\gamma$* )

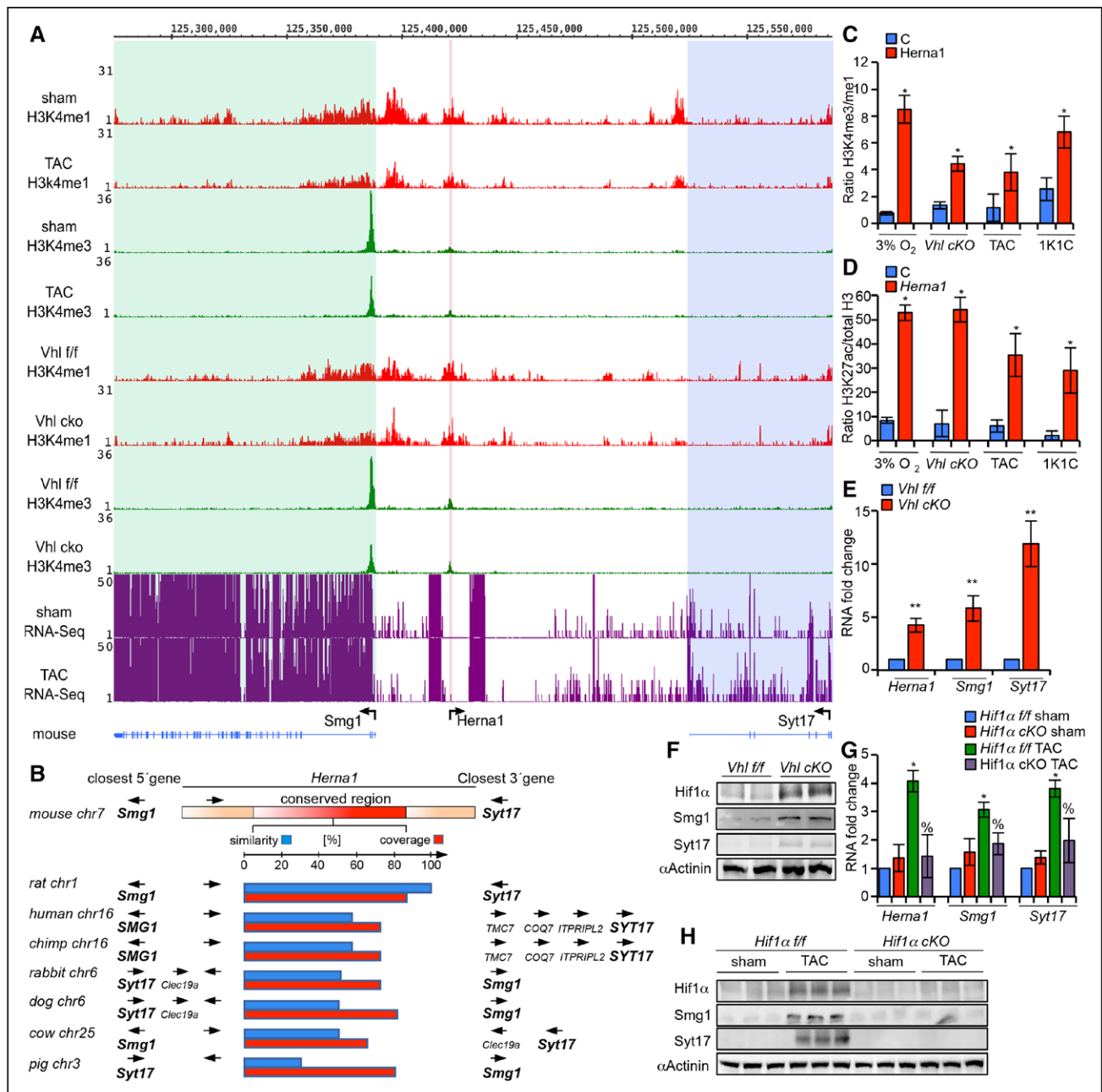


**Figure 1. *Herna1* identification and functional relevance.**

**A**, UCSC Genome Browser (mm9 assembly) presentation of H3K4me1 and H3K4me3 modifications obtained from ChIP-Seq analyses at the *Herna1* genomic locus (labeled with vertical pink stripe) in sham, TAC, *Vhl f/f*, and *Vhl c/o* cardiac left ventricle and RNA transcript generation based on RNA-Seq profiles. **B**, Conservation of the *Herna1* loci and its flanking regions across species. **C**, Samples described in **A**, and left ventricular samples from 1-Kidney/1-Clip experiments, as well, were subjected to targeted ChIP analyses with antibodies against H3K4me3 and H3K4me1. H3K4me3 abundance within the indicated genomic regions was calculated as the ratio between H3K4me3 and H3K4me1. **D**, Samples described in **A**, and left ventricular samples from 1-Kidney/1-Clip experiments, as well, were subjected to targeted ChIP analyses with antibodies against total H3 and H3K27ac. H3K27ac abundance within the indicated genomic regions was calculated as the ratio between H3K27ac and total H3. **E**, *Vhl f/f* and *Vhl c/o* left ventricular biopsies were assessed for *Herna1*, *Smg1*, and *Syt17* RNA expression, normalized to *Hprt1* mRNA; two-tailed unpaired *t* test. **F**, *Vhl f/f* and *Vhl c/o* left ventricular biopsies were assessed for Hif1 $\alpha$ , Smg1, and Syt17 protein expression (normalized to sarcomeric  $\alpha$ -actinin). **G**, *Hif1 $\alpha$  f/f* and *Hif1 $\alpha$  c/o* mice subjected to sham or TAC were assessed for *Herna1*, *Smg1*, and *Syt17* RNA expression, normalized to *Hprt1* mRNA (\**P*<0.05 compared with *Hif1 $\alpha$  f/f* sham; %*P*<0.05 compared with *Hif1 $\alpha$  f/f* TAC; 2-way ANOVA with Tukey post hoc test). **H**, *Hif1 $\alpha$  f/f* and *Hif1 $\alpha$  c/o* mice subjected to TAC were assessed for Hif1 $\alpha$ , Smg1, and Syt17 protein expression in cardiac left ventricle (normalized to sarcomeric  $\alpha$ -actinin). Error bars indicate SD of the mean (**C**, **D**). Error bars indicate SE of the mean (**E**, **G**). *n* = 3 biological replicates per group. **C** through **E**, \**P*<0.05; \*\**P*<0.01 2-tailed unpaired *t* test. ChIP-Seq indicates chromatin immunoprecipitation–coupled sequencing; H3K4me1, histone 3 lysine 4 monomethylation; H3K4me3, trimethylated histone H3 lysine 4; RNA-Seq, RNA sequencing; and TAC, transaortic constriction.

promoter void of enhancer features. Finally, to confirm the innate capacity of *Herna1* to increase target gene expression, we used the  $\kappa$ N–BoxB tethering-based re-

porter assay.<sup>21</sup> A chimeric RNA containing *Herna1* fused to *BoxB* RNA was engineered to facilitate recruitment of the *BoxB*–*Herna1* RNA fusion to the RNA binding domain

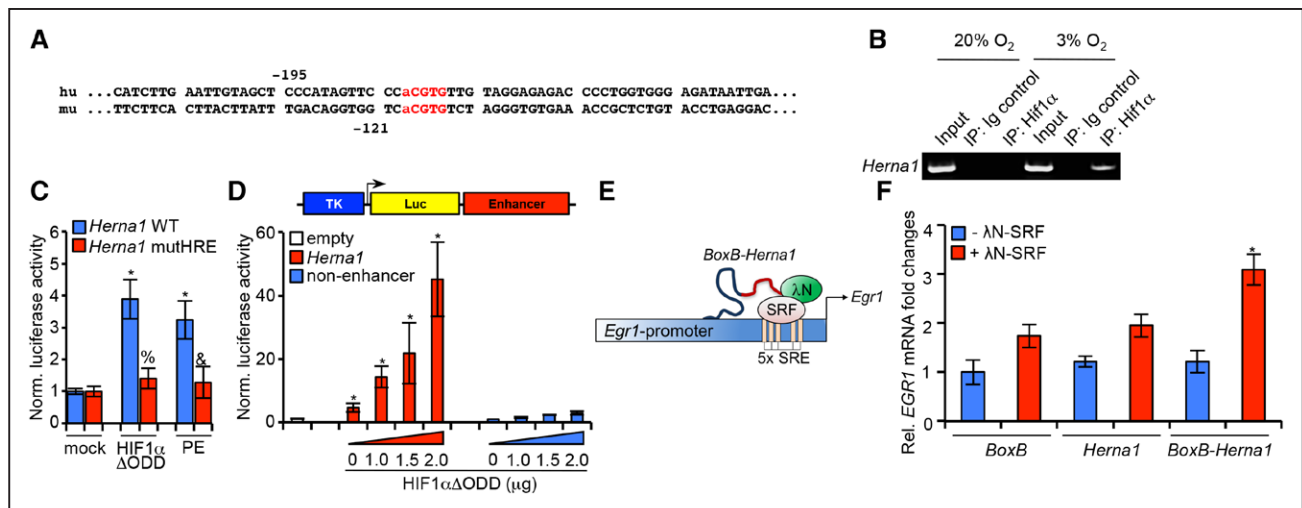


**Figure 2. Herna1 is a HIF1 $\alpha$ -dependent noncoding RNA with enhancer function.**

**A**, Sequence of the human and mouse *Herna1* promoter. Conserved hypoxia responsive element (HRE) is shown in red, with the core HRE motif capitalized. **B**, NMCs cultured at 20% O<sub>2</sub> or 3% O<sub>2</sub> and assessed for chromatin immunoprecipitation of the *Herna1* promoter with a HIF1 $\alpha$ -specific antibody (IP: HIF1 $\alpha$ ) or with a control isotype-matched antibody (IP: IgG control). **C**, Hif1 $\alpha$ -dependent *Herna1* promoter activity was determined by transient transfection of wild-type or HRE-mutated *Herna1* promoter, respectively, fused to luciferase and with either an empty vector control, HIF1 $\alpha$ ΔODD or PE stimulation, and cotransfection with a  $\beta$ -galactosidase construct for normalization of luciferase signal. \* $P$ <0.05 in comparison with mock/*Herna1* WT promoter transfected NMCs; % $P$ <0.05 in comparison with HIF1 $\alpha$ ΔODD treated and *Herna1* WT promoter transfected NMCs; & $P$ <0.05 in comparison with PE treated and *Herna1* WT promoter transfected NMCs. Two-way ANOVA with Tukey post hoc test. **D**, 3 kb of the genomic region flanking the *Herna1* transcript was assessed for enhancer activity in response to HIF1 $\alpha$  by transient transfection of *Herna1* fused to SV-40 luciferase, and transfection with an empty vector control or HIF1 $\alpha$ ΔODD at increasing concentrations, and cotransfection with a  $\beta$ -galactosidase construct for normalization of luciferase signal. The *Ppar $\gamma$*  promoter serves as control. \* $P$ <0.05 in comparison with empty-vector control, 1-way ANOVA with Dunnett post hoc test. **E**, Schematic diagram of the *Herna1*-BoxB- $\lambda$ N tethering system. **F**, *Egr1* mRNA expression was assessed by qPCR after cotransfection of *Herna1*-BoxB with the  $\lambda$ N-SRF fusion construct in 293T cells. Data were normalized to *Hprt1*. **C**, **D**, and **F**,  $n$ =3 to 4 biological replicates per group. Error bars indicate SD of the mean. \* $P$ <0.05 *Herna1*-BoxB+ $\lambda$ N-SRF in comparison with all others (**F**). Two-way ANOVA with Tukey post hoc test. HIF1 $\alpha$  indicates hypoxia-inducible factor 1 $\alpha$ ; HRE, hypoxia-response element; NMC, neonatal mouse cardiomyocyte; PE, phenylephrine; qPCR, quantitative polymerase chain reaction; SRF, serum response factor; and WT, wild-type.

of  $\lambda$ N protein fused to the serum response factor (Srf) gene ( $\lambda$ N-Srf; Figure 2E). Thus, *Herna1* can be artificially tethered to serum response factor transcription factor response elements within the early growth response gene 1 (*Egr1*) promoter (Figure 2E).<sup>22</sup> We observed that the BoxB-*Herna1* RNA fusion increased *Egr1* mRNA expression in comparison with transfection of either BoxB or *Herna1* alone (Figure 2F and Figure IVK and IVL in the online-only Data Supplement). These data support the fact that the *Herna1* transcript itself directs flanking gene transcription on Hif1 $\alpha$ -induced activation, and is consistent with the functional mechanism of a documented estrogen receptor  $\alpha$  eRNA.<sup>10</sup>

Given that *Herna1* expression parallels that of *Smg1* and *Syt17*, we asked if the *HERNA1* transcript interacts with the promoters of *Smg1* and *Syt17* to drive transcription. Hence, we quantified *HERNA1* binding at the *Smg1* and *Syt17* promoter by chromatin isolation by RNA purification (ChIRP),<sup>23</sup> using glyceraldehyde-3-phosphate dehydrogenase (*Gapdh*) and nuclear paraspeckle assembly transcript 1 (*Neat1*), established coding and noncoding hypoxia targets,<sup>24,25</sup> as promoter controls for the efficiency and specificity of *Herna1* interaction (Figure 3A and 3B). Despite pronounced hypoxia-induced *Gapdh* and *Neat1* expression (Figure 3A), *Herna1* binding was not detected at the *Gapdh* or *Neat1* promoters but mainly at the *Smg1* and *Syt17*

promoters (Figure 3B), suggestive of selective *Herna1* interaction at these promoters. Next, we subdivided the *Smg1* and *Syt17* promoters into three 500-kb domains and assessed interactions of the respective RNAs by ChIRP-quantitative polymerase chain reaction (Figure 3C). *Gapdh* and *Neat1* ChIRP pull-down products served as specificity controls for *Herna1* interactions. A clear signal was detected for *Herna1* at the *Smg1* and *Syt17* promoters between -1000 and -500 bp and -1000 and 0 bp upstream of the respective transcription start site (Figure 3C). ChIRP pull-down of *Gapdh* and *Neat1* RNA did not reveal such robust interactions at the *Smg1* (Figure 3C, upper) or *Syt17* promoters (Figure 3C, lower). Fluorescence in situ hybridization for *Herna1* and its flanking genes revealed coregulation and colocalization of all transcripts from the *Smg1*-*Herna1*-*Syt17* gene cluster in isolated cardiomyocytes cultured at 3% O<sub>2</sub> (Figure 3D). These results suggest that *Herna1* acts at nearby genes to promote their transcriptional activation in a hypoxia-dependent manner.

### HERNA1 Is Necessary for Pathology-Induced Smg1 and Syt17 Activity

We generated short-hairpin RNAs (shRNAs) targeting mouse *Herna1* (shHerna1), of which 2 individual clones efficiently inhibited hypoxia-induced *Herna1* expression,

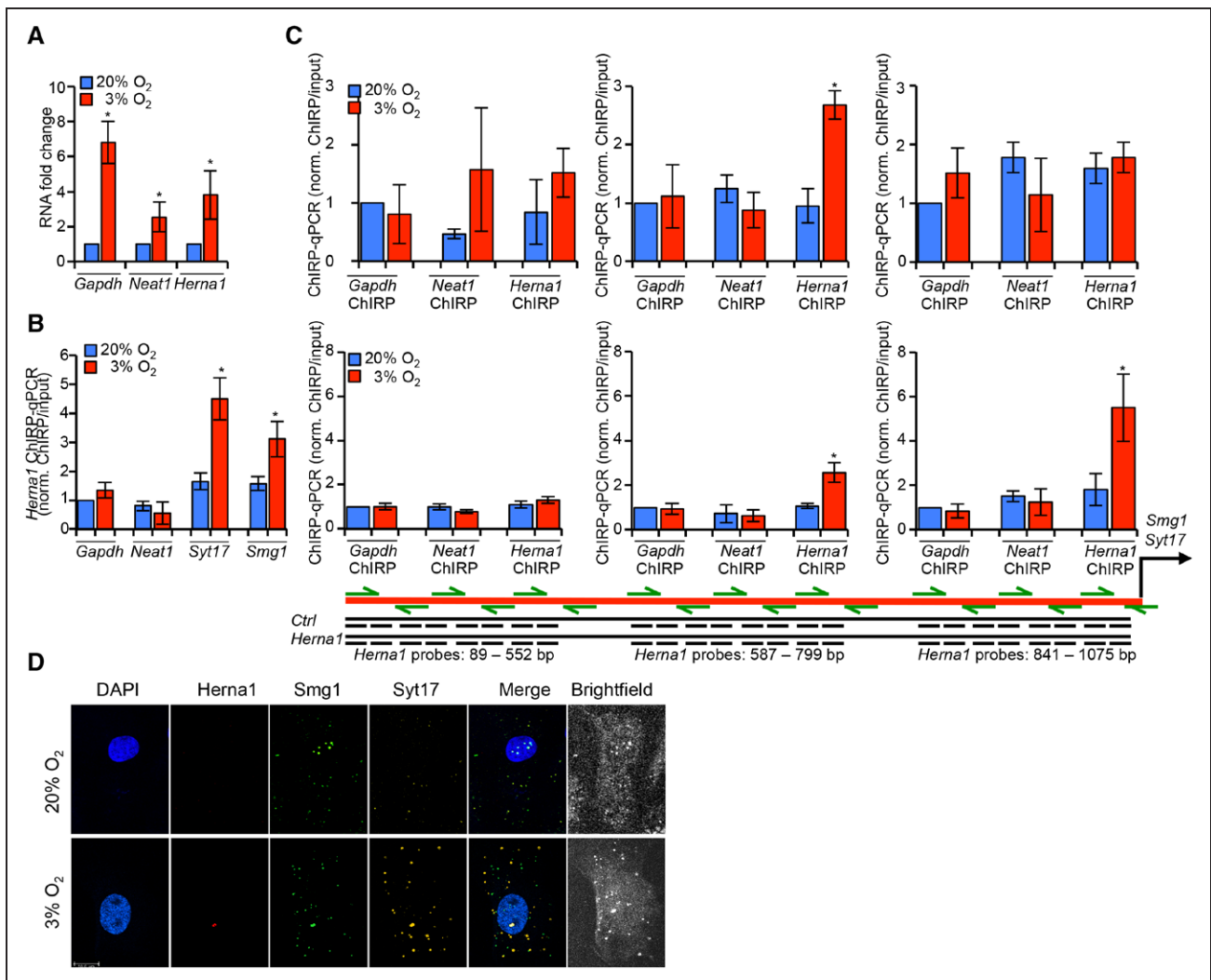


**Figure 3. Herna1 binds at the promoter of neighboring genes Syt17 and Smg1.**

**A**, NMCs cultured as shown were assessed for *Gapdh*, *Neat1*, and *Herna1* RNA by RT-qPCR and normalized to *Hprt1*. **B**, *Herna1* interaction at the *Smg1* and *Syt17* promoter in hypoxia and normoxia was assessed by ChIRP-qPCR by using promoter-specific primers. *Gapdh* and *Neat1* promoter qPCR serve as controls. **C**,  $\sim 1.5$  kb of the *Smg1* (**Top**) and *Syt17* (**Bottom**) promoter was divided into 3 domains ( $-1500$  to  $-1000$  bp,  $-1000$  to  $-500$  bp and  $-500$  to  $0$  bp) and assessed by qPCR for *Herna1* interaction. ChIRP pull-down of *Gapdh* and *Neat1* RNA serve as controls. **D**, Representative images of *Herna1*, *Smg1*, and *Syt17* RNA localization under normoxia and hypoxia as determined by RNA-FISH. Nuclei were stained with DAPI. Scale bar is  $100 \mu\text{m}$ . **A** through **C**,  $*P < 0.05$ ; multiple 2-sample *t* test in comparison with NMCs treated in  $20\% \text{O}_2$ ,  $n=3$  biological replicates per group. Error bars indicate SD of the mean. ChIRP indicates chromatin isolation by RNA purification; DAPI, 4',6'-diamidino-2-phenylindole; FISH, fluorescence in situ hybridization; NMC, neonatal mouse cardiomyocyte; and RT-qPCR, quantitative reverse transcription polymerase chain reaction.

resulting in the concordant downregulation of *Smg1* and *Syt17* in NMCs on the RNA and protein level (Figure 4A and 4B). In line with *Smg1* repression, phosphorylation of its substrate *Upf1* was abolished (Figure 4B). Next, we assayed for *Herna1*-mediated cell growth by [ $^3\text{H}$ ]leucine incorporation and cell size quantification in NMCs subjected to either hypoxia, dimethylxaloylglycine (a chemical inhibitor of prolyl hydroxylases), PE stimulation, or ectopic HIF1 $\alpha\Delta\text{ODD}$  expression. *Herna1* depletion suppressed pathological stress-induced cell growth (Figure 4C and Figure VA through VC in the online-only Data Supplement), suggesting that *Herna1* mediates the pathological growth response through Hif1 $\alpha$ . Transition to pathology occurs concomitant with increased glucose utilization and dependence, reduced oxidative phosphorylation

capacity, and repressed cardiomyocyte contractility.<sup>16</sup> To interrogate *Herna1* function in these contexts, NMCs expressing ectopic HIF1 $\alpha\Delta\text{ODD}$  were transduced with sh*Herna1* and kinetic analysis of glycolytic and fatty acid oxidation rates was determined. As noted in Figure 4D and 4E, ectopic HIF1 $\alpha\Delta\text{ODD}$  expression led to increased glycolysis, and repression of fatty acid oxidation and maximal respiratory capacity, as readout for mitochondrial respiratory function. However, on simultaneous *Herna1* inactivation, the shift to glycolysis at the expense of fatty acid oxidation and mitochondrial function was severely attenuated (Figure 4F and 4G). A similar response was observed in dimethylxaloylglycine, isoproterenol, or PE-treated NMCs on sh*Herna1* infection (Figure VD and VE in the online-only Data Supplement). sh*Herna1* treatment

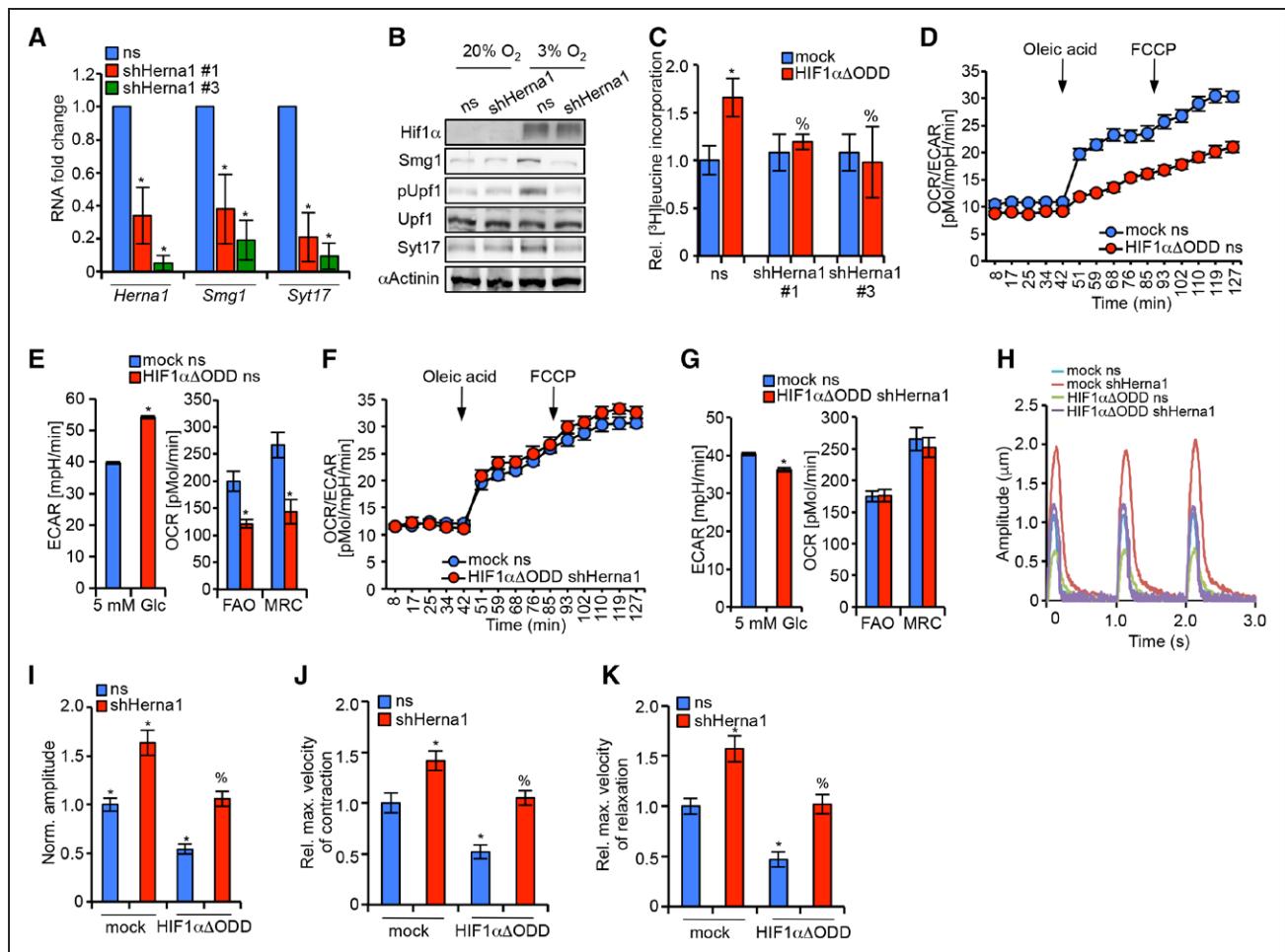


**Figure 4.** *Herna1* expression levels affect expression of *Smg1* and *Syt17* as well as cellular growth and contractility.

**A**, NMCs were subjected to 3%  $O_2$  and transduced with ns or 2 unique shRNAs targeting *Herna1* and assessed for *Herna1*, *Smg1*, and *Syt17* RNA, normalized to *Hprt1* ( $*P < 0.05$  in comparison with ns-treated NMCs; 1-way ANOVA with Dunnett post hoc test). **B**, NMCs cultured as indicated and in the presence of nonsilencing shRNA (ns) or shRNA targeting *Herna1* were assessed for denoted protein levels. Loading is normalized to sarcomeric  $\alpha$ -actinin. **C**, NMCs stimulated with ectopic HIF1 $\alpha$  $\Delta$ ODD in combination with a control ns or 2 unique shRNAs targeting *Herna1* were assessed for [ $^3$ H]leucine incorporation.  $*P < 0.05$  in comparison with ns/mock-treated NMCs,  $\%P < 0.05$  in comparison with ns/ HIF1 $\alpha$  $\Delta$ ODD treated NMCs, 2-way ANOVA with Tukey post hoc test. **D** through **G**, Assessment of extracellular acidification rate (ECAR), and oleic acid- and carbonyl cyanide-4 (trifluoromethoxy)-phenylhydrazone (FCCP)-induced oxygen consumption rate (OCR) in NMCs transduced and treated as indicated. Depicted are rates expressed as OCR to ECAR ratios (**D** and **F**), and quantified ECAR and OCR values (**E** and **G**). FAO and MRC indicate fatty acid oxidation rate and mitochondrial respiratory complex capacity, respectively.  $*P < 0.05$  in comparison with ns/mock-treated NMCs, paired *t* test. **H** through **K**, NMCs expressing HIF1 $\alpha$  $\Delta$ ODD in combination with ns or shHerna1 were stimulated at 1 Hz and assessed for contractile amplitude. **H**, Shows representative traces; **I**, quantified contractile amplitude; **J** and **K**, relative maximal velocity of contraction and relaxation.  $*P < 0.05$  in comparison with ns/mock treatment,  $\%P < 0.05$  in comparison with HIF1 $\alpha$  $\Delta$ ODD ns treatment, 2-way ANOVA with Tukey post hoc test. **A**, **C**, **H** through **K**,  $n = 3$  biological replicates per group. Error bars indicate SD of the mean. **D** through **G**,  $n = 8$  biological replicates per group. Error bars indicate SE of the mean. Mock-transduced samples were used to control HIF1 $\alpha$  $\Delta$ ODD treatment. HIF1 $\alpha$  indicates hypoxia-inducible factor 1 $\alpha$ ; HIF1 $\alpha$  $\Delta$ ODD, HIF1 $\alpha$  lacking the oxygen-dependent degradation domain; and NMC, neonatal mouse cardiomyocyte.

also reverted the contractile defects associated with pathological transition, revealing a beneficial positive inotropic and lusitropic effect of *Herna1* inhibition both at the basal state and on HIF1 $\alpha$  $\Delta$ ODD expression (Figure 4H through 4K). These data reveal a requirement of *Herna1* function in mediating the maladaptive growth, metabolic, and contractile changes associated with pathology.

## Smg1 and Syt17 Drive Distinct Aspects of Pathological Transition

Little is known about *Smg1* and *Syt17* function in cardiomyocytes. We characterized the subcellular lo-

calization of the respective proteins in NMCs. *Smg1* is primarily localized in the nuclei of cardiomyocytes, whereas *Syt17* colocalizes with *Atp5a1* (a core component of ATP Synthase/Complex V), indicative of mitochondrial localization (Figure 5A and 5B). Based on these findings and the fact that *Smg1* and *Syt17* are targets of *Herna1*, we identified shRNAs inhibiting *Smg1* and *Syt17* expression effectively at the RNA and protein level (Figure 5C and 5D and Figure VIA and VIB in the online-only Data Supplement). These shRNAs were transduced into cells subjected to hypoxia, ectopic HIF1 $\alpha$  $\Delta$ ODD expression, or PE stimulation. Depletion of *Smg1* and *Syt17* in these contexts prevented

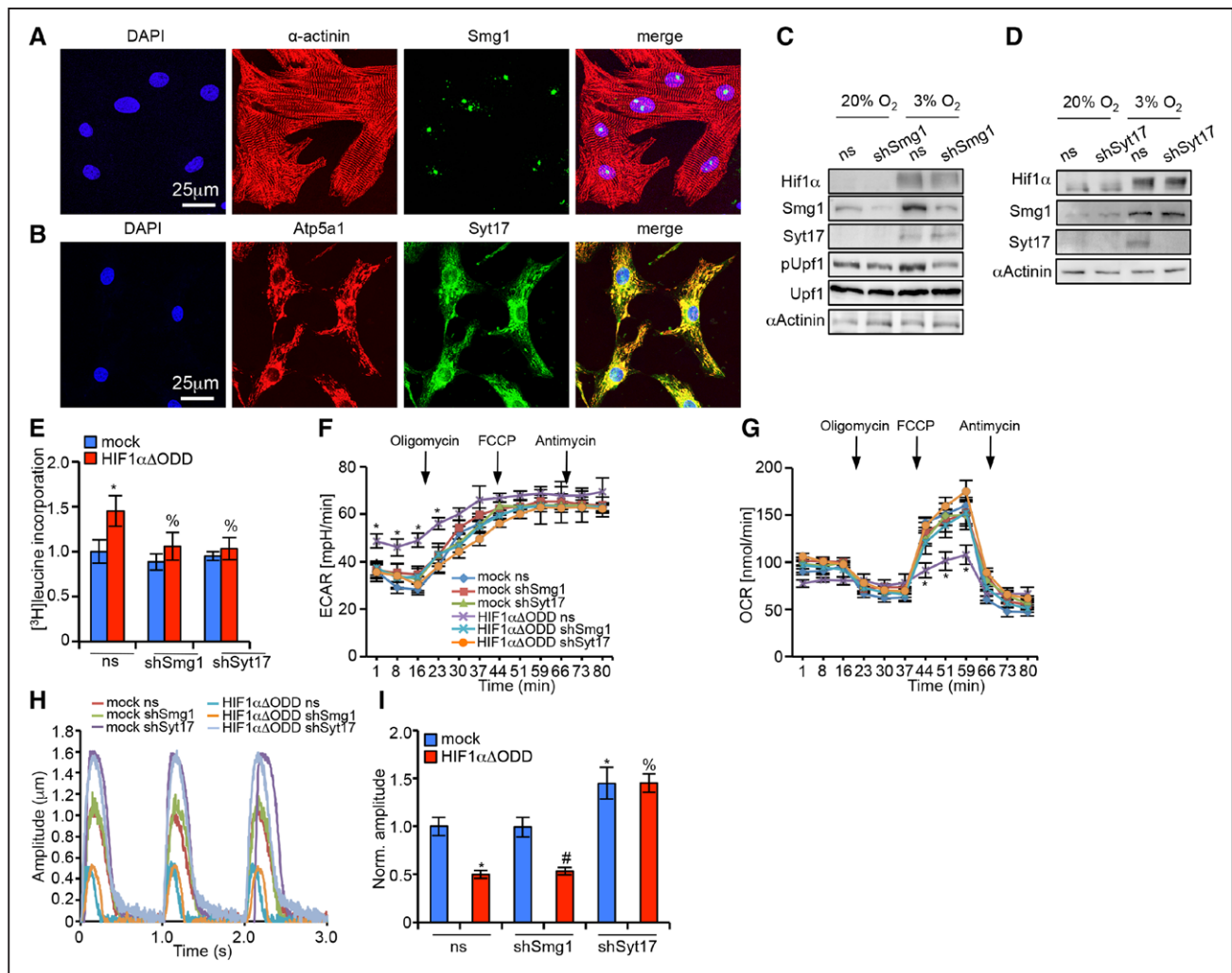


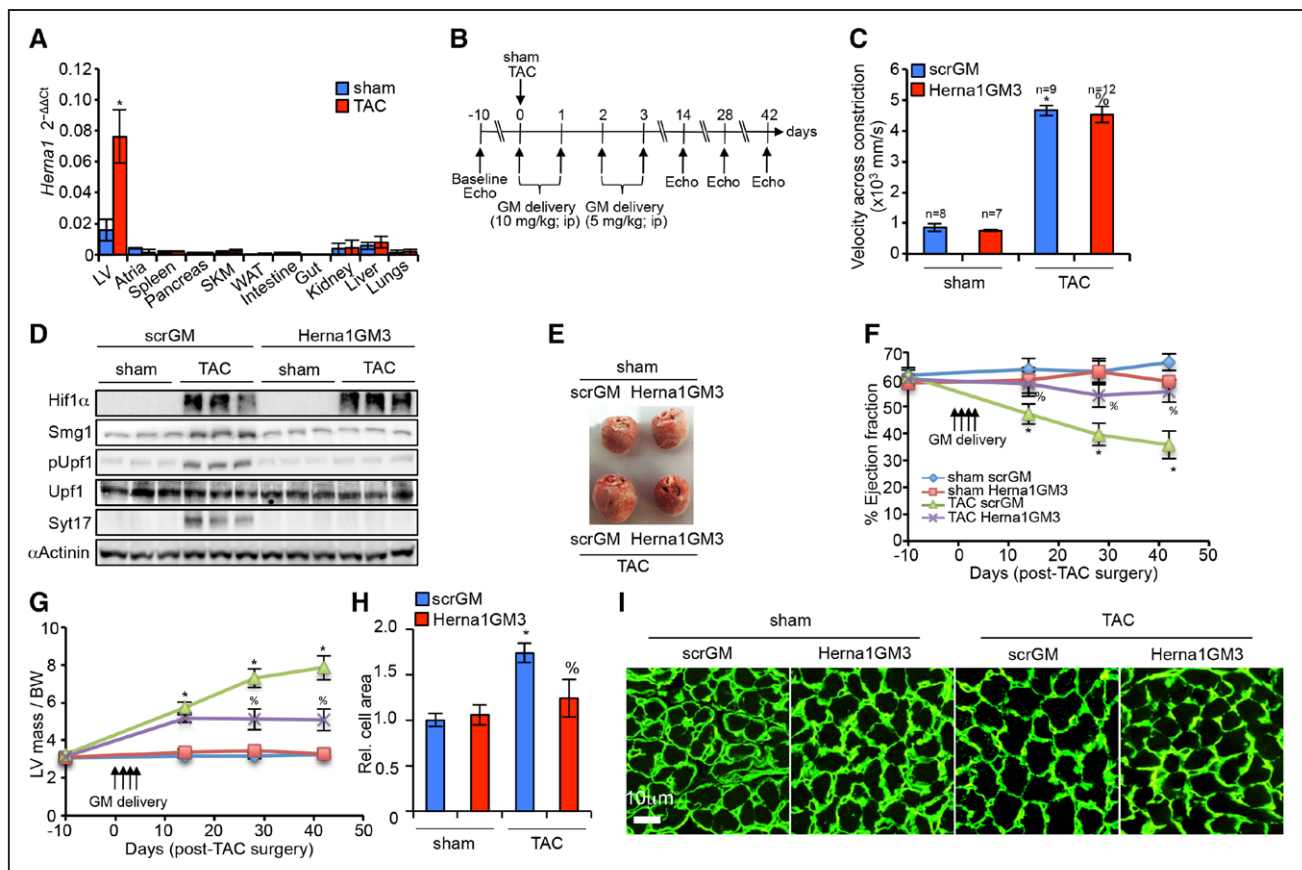
**Figure 5. Smg1 and Syt17 expression affects cardiomyocyte growth under pathological stress, whereas contractility is mainly regulated by Syt17.** **A**, NMCs were stained for cardiomyocyte-specific  $\alpha$ -actinin, Smg1, and DAPI, and imaged by confocal microscopy. Representative fields are shown. Scale bar, 25  $\mu$ m. **B**, NMCs were stained for the mitochondrial marker Atp5a1, Syt17, and DAPI, and imaged by confocal microscopy. Representative fields are shown. Scale bar, 25  $\mu$ m. **C** and **D**, NMCs cultured in 20%  $O_2$  or 3%  $O_2$  in the presence of nonsilencing shRNA (ns) or shSmg1 (**C**) or shSyt17 (**D**), were assessed for denoted protein levels by immunoblotting. Loading is normalized to sarcomeric  $\alpha$ -actinin. **E**, NMCs transduced with empty control or ectopic HIF1 $\alpha$ ODD in combination with ns, shSmg1, or shSyt17 were assessed for [ $^3$ H]leucine incorporation. (n=3 biological replicates per group). Error bars indicate SD of the mean \* $P$ <0.05 in comparison with ns/mock treatment, % $P$ <0.05 in comparison with ns/HIF1 $\alpha$ ODD treatment, 2-way ANOVA with Tukey post hoc test). **F** and **G**, NMCs expressing ectopic HIF1 $\alpha$ ODD in combination with ns, shSmg1, or shSyt17 were assessed at the baseline state, after an injection of oleic acid and FCCP. Mock transduced samples serve as controls. Depicted are ECAR (**F**) and OCR (**G**) rates at the respective time-Herna1s. (n=8 biological replicates per group). Error bars indicate SE of the mean. **H** and **I**, NMCs treated as in **F** and **G**, were stimulated at 1 Hz and assessed for contractile amplitude. Representative traces are shown in **H**, and contractile amplitude in **I** (n=3 biological replicates per group). Error bars indicate SD of the mean. **F**, **G**, and **I** \* $P$ <0.05 in comparison with ns/mock treatment, # $P$ <0.05 in comparison with shSmg1/mock treatment; % $P$ <0.05 in comparison with HIF1 $\alpha$ ODD ns treatment, 2-way ANOVA for repeated measures with Tukey post hoc test. DAPI indicates 4',6-diamidino-2-phenylindole; ECAR, extracellular acidification rate; FCCP, carbonyl cyanide-4 (trifluoromethoxy)-phenylhydrazone; HIF1 $\alpha$ , hypoxia-inducible factor 1 $\alpha$ ; HIF1 $\alpha$ ODD, HIF1 $\alpha$  lacking the oxygen-dependent degradation domain; NMC, neonatal mouse cardiomyocyte; and OCR, oxygen consumption rate.

a hypertrophic cell growth response (Figure 5E and Figure VIC through VIF in the online-only Data Supplement), indicating that Hif1 $\alpha$ -Herna1-Smg1/Syt17 axis promotes pathological stress-induced cardiomyocyte growth. Moreover, metabolic analysis of NMCs depleted for Smg1 or Syt17 in combination with either HIF1 $\alpha$ ODD overexpression or treatment with dimethylxaloylglycine, isoproterenol, or PE revealed a requirement of Smg1 or Syt17 for efficient reprogramming of cardiomyocyte metabolism toward glycolysis, in the context of stressors activating HIF signaling

(Figure 5F and 4G and Figure VIG through VII in the online-only Data Supplement). In contrast to the function of both Smg1 and Syt17 in pathological growth and metabolism, only Syt17 regulates contractile function. Cardiomyocytes treated with shRNAs against Syt17 abolished the HIF1 $\alpha$ ODD-induced decrease in contractile amplitude, maximal velocity of contraction and relaxation (Figure 5H and 5I and Figure VIJ and VIK in the online-only Data Supplement), whereas Smg1 inactivation did not affect HIF1 $\alpha$ ODD-mediated contractile repression.

To identify downstream molecular changes dependent on Smg1 or Syt17, we performed RNA sequencing and analyzed differential gene expression on cardiomyocytes cultured in normoxia or hypoxia, concomitant to Smg1 or Syt17 inactivation. To simplify the data, we isolated gene subsets that were induced or repressed in hypoxia (relative to normoxia nsRNA controls) but normalized by either Smg1 or Syt17 inactivation. In categorizing these differentially expressed genes, we identified specific gene subsets that directly inhibit the hypoxia-driven growth, metabolic, and contractile maladaptation. As noted in [Figure VIIA in the online-only Data Supplement](#), expression of a larger gene subset was normalized to control levels by Smg1 inactivation (in comparison to Syt17). Functional clustering of genes normalized by both Smg1 and Syt17 inactivation

revealed an enrichment for genes implicated in growth and metabolic control ([Figure VIIB in the online-only Data Supplement](#)), whereas individually, Smg1 and Syt17 inactivation also led to the normalization of specific metabolism and growth genes ([Figure VIIC and VIID in the online-only Data Supplement](#)). Consistent with our in vitro contractility analysis, Syt17 knockdown led to expression normalization of genes linked to cardiomyocyte contractility ([Figure VIIE in the online-only Data Supplement](#)). To confirm these effects, Serca2 and Phospholamban phosphorylation was analyzed in NMCs cultured in normoxia or hypoxia and transduced with shNs or shSyt17. Hypoxia led to a clear downregulation of Serca2 expression and reduced Phospholamban phosphorylation in shNs transduced NMCs, whereas Serca2 expression was increased on shSyt17 depletion



in normoxia and hypoxia (Figure VIIF in the online-only Data Supplement). Thus, *Herna1*-dependent *Smg1* and *Syt17* expression in response to stressors engages, at a minimum, 2 pathways with distinct roles in cardiomyocyte growth, metabolism, and contractility regulation.

## Herna1 Inactivation Attenuates Disease Development In Vivo

Enhancers modulate spatiotemporal gene expression and enhancer-associated RNAs can exhibit tissue- and context-specific gene expression.<sup>26</sup> Thus, we assessed *Herna1* tissue distribution in mice subjected to aortic stenosis-induced hypertrophy (TAC) mimicking pressure overload as seen in aortic stenosis or hypertrophic obstructive cardiomyopathies. As noted in the quantitative polymerase chain reaction analysis, *Herna1* expression was elevated in the left ventricle of mice only on TAC, whereas expression in other tissues remained low both in sham and TAC-treated mice (Figure 6A). To define *Herna1* function in vivo, we screened for ASO gapmers that would efficiently target *Herna1* for degradation in NMCs ectopically expressing HIF1 $\alpha$  $\Delta$ ODD (Figure VIIIA in the online-only Data Supplement). Gapmers are chimeric ASOs that contain a central block of deoxynucleotide monomers to induce RNaseH cleavage.<sup>27</sup> *Herna1* gapmers inhibited hypoxia-induced *Smg1* and *Syt17* expression in NMCs, suppressed hypertrophy on ectopic HIF1 $\alpha$  $\Delta$ ODD or PE stimulation, and rescued Hif1 $\alpha$ -mediated contractile inhibition (Figure VIIIB through VIIID in the online-only Data Supplement). These gapmers were then applied in TAC experiments to investigate potential contributions of *Herna1* to hypertrophic heart disease development. Scrambled and *Herna1*-targeting gapmers were delivered before TAC surgery and for the next 3 consecutive days as depicted in Figure 6B. The mice were assessed for 42 days post-TAC with echocardiography performed at regular 14-day intervals. TAC surgery led to a comparable increase in aortic flow velocity in the respective TAC groups (Figure 6C). Consistent with effects in vitro, *Herna1*GM3 delivery in mice resulted in blunted *Herna1* levels, reduced *Smg1* and *Syt17* expression, and attenuated phosphorylation of *Upf1* (Figure 6D and Figure VIIIE in the online-only Data Supplement). Mice subjected to TAC and treated with scrGM exhibited pronounced decline in cardiac function, increased hypertrophy and ventricular dilatation from 14-days post-TAC (Figure 6E through 6I and Figure VIIF and VIIIF in the online-only Data Supplement). In contrast, TAC mice treated with *Herna1*GM3 exhibited a blunted response to the induction of ventricular dilatation and hypertrophy, while maintaining cardiac function up to 42-days post-TAC surgery (Figure 6F and 6G and Figure VIIIG and VIIIG in the online-only Data Supplement). These findings were recapitulated by using an independent *Herna1*-targeting ASO gapmer,

*Herna1*GM1 (Figure VIIIF through VIIIF in the online-only Data Supplement). Hence, *Herna1* function is critical for the development of pathological stress-induced hypertrophic heart disease.

Next, we interrogated *Herna1* function in mice exhibiting overt indications of pathological growth, dilatation, and contractile dysfunction to evaluate the therapeutic implications of *Herna1* inhibition. C57Bl/6 mice were randomly assigned into 2 groups, with the groups subjected to either sham or 1K1C surgery and further subdivided for scrGM or *Herna1*GM3 treatment on pathology development (Figure 7A). The 1K1C protocol leads to cardiomyopathy subsequent to the development of hypertension.<sup>28,29</sup> 1K1C surgery was performed and hypertrophy allowed to progress until overt indications of cardiac dysfunction were observed by echocardiography, at which time gapmer treatment was initiated and echocardiography was performed at regular intervals to monitor disease progression (Figure 7A). Blood pressure was assessed to confirm the elevation on 1K1C surgery (Figure 7B). In line with TAC experiments *Herna1* expression was only elevated in cardiac left ventricle of mice on hypertension-induced pressure overload (Figure 7C). *Herna1*GM3 led to the inhibition of pathology-induced *Herna1*, *Syt17*, *Smg1* expression and reduced *Upf1* phosphorylation (Figure 7D and Figure IXA in the online-only Data Supplement). At 56 days post-1K1C, cardiac dysfunction was observed in the 1K1C group and mice from the respective groups were further subdivided for scrGM or *Herna1*GM3 therapy. After disease progression by echocardiography, 1K1C-operated mice treated with scrGM displayed progressive decline in cardiac function as evidenced by ventricular dilatation and reduced cardiac ejection fraction throughout the 91-day duration (Figure 7E through 7G and Figure IXB through IXD in the online-only Data Supplement). However, 1K1C mice treated with *Herna1*GM3 demonstrated resolution of disease-associated pathologies including gradual improvement of cardiac function and reversion of hypertrophic cardiac growth (Figure 7F and 7G and Figure IXB through IXD in the online-only Data Supplement). It is notable that, despite the protection conferred by *Herna1*GM3 in 1K1C mice, a mild increase in physical heart weight was detected at the end of the protocol (Figure 7G), although this was not reflected in 2-dimensional surface area measurements of cardiomyocytes from these hearts (Figure 7H and 7I). Consistent with the echocardiography measurements, mice from the 1K1C scrGM-treated group displayed reduced overall survival in comparison with 1K1C mice treated with *Herna1*GM3 (Figure 7J). These findings were confirmed by using an independent *Herna1*-targeting ASO gapmer, *Herna1*GM1 (Figure IXE through IXH in the online-only Data Supplement). Thus, pathological stress-induced *Herna1* expression is critical for

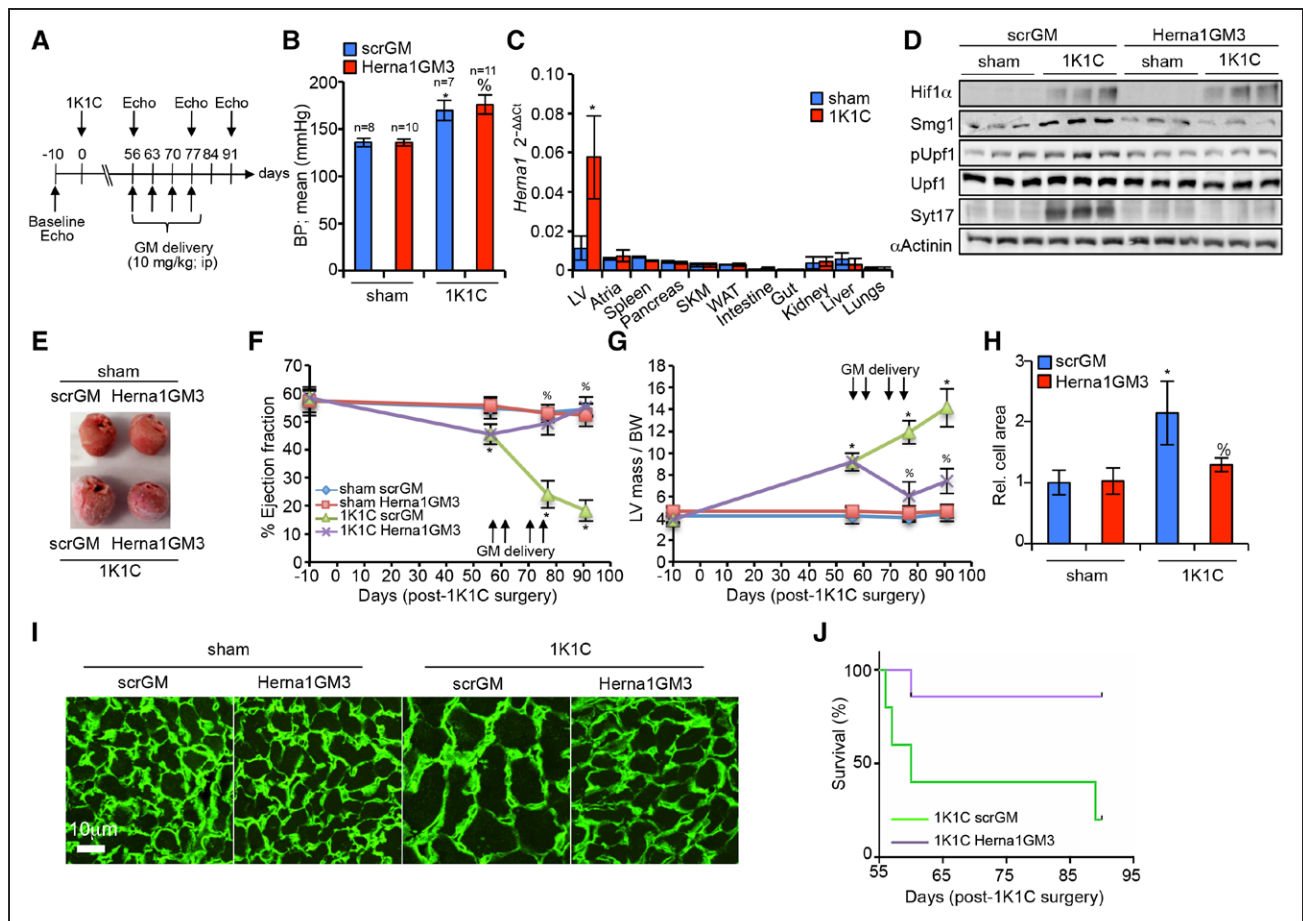


**Figure 7. Herna1 inactivation is a potential therapeutic target in pressure overload-induced cardiac hypertrophy.**

**A**, Schematic representation of the 1K1C protocol. Gapmer dosage, delivery time-Herna1s, and longitudinal echocardiography monitoring was performed as indicated. **B**, Mean blood pressure of mice treated as described in **A** is shown (\* $P < 0.05$ ; in comparison with scrGM sham; % $P < 0.05$  in comparison with Herna1GM3 sham 2-way ANOVA with Tukey post hoc test). **C**, RNA derived from indicated tissues of mice subjected to sham or 1K1C surgery was assessed for *Herna1* by qPCR. All values were normalized to *Hprt1* mRNA. Error bars indicate SE of the mean. \* $P < 0.05$  in comparison with expression in sham, multiple 2-sample  $t$  test. **D**, Left ventricular biopsies of sham and 1K1C-operated mice treated with control scrGM or Herna1GM3 as described in **A**, were assessed for denoted proteins, sarcomeric  $\alpha$ -actinin was used as loading control. **E**, Whole hearts harvested from mice, as described in **A**, were harvested and imaged. **F** and **G**, Longitudinal monitoring of cardiac % ejection fraction (%EF; **F**) and echocardiography quantified left ventricular weight normalized to body weight (**G**) of sham- or 1K1C-operated mice treated with scrGM or Herna1GM3. Arrows in panels indicate gapmer injections as described in **A**. \* $P < 0.05$  in comparison with scrGM sham; % $P < 0.05$  in comparison with 1K1C scrGM, 2-way ANOVA for repeated measures with Tukey post hoc test. **H**, Cell area quantification of laminin-stained histological sections of mice hearts after 13 weeks of sham or 1K1C surgery, treated with scrambled or Herna1 gapmers. \* $P < 0.05$  in comparison with scrGM sham; % $P < 0.05$  in comparison with scrGM 1K1C 2-way ANOVA with Tukey post hoc test. **I**, Representative images of histological sections described in **H**. **J**, Kaplan–Meier survival curves of denoted mice. Because of the absence of mortality in the sham groups, sham group data are not shown for clarity. **C**, **H**, and **I**,  $n = 3$  mice per group; 1-way ANOVA followed by a Dunnett multiple-comparison post hoc test. **B**, **F**, **G**, and **J**,  $n = 8$  mice for sham scrGM,  $n = 10$  for sham Herna1GM3,  $n = 7$  for 1K1C scrGM,  $n = 11$  for 1K1C Herna1GM3. Error bars indicate SE of the mean. BP indicates blood pressure; BW, body weight; 1K1C, 1 kidney 1-clip; LV, left ventricle; qPCR, quantitative polymerase chain reaction; SKM, skeletal muscle; and WAT, white adipose tissue.

maintaining key aspects of hypertrophic heart disease-associated pathologies in mouse models.

## Herna1 Function Can Be Uncoupled Via Smg1 and Syt17 In Vivo

In vitro phenotypic analysis and gene expression profiling of Smg1 and Syt17 function revealed cooperation of both genes in normalizing cardiomyocyte hypertrophy and metabolism, but a unique capacity of Syt17 in correcting the maladaptive contractility induced by stress (Figure 5H and 5I and Figure VII E and VIIF in the online-only Data Supplement). To assess if these *Herna1*-flanking genes confer similar effects in vivo, we

subjected mice expressing Cre recombinase under the control of the ventricle-specific *myosin light chain 2v* (*MLC2v*) promoter (*MLC2v-cre*<sup>+30</sup>) to TAC and delivered a modified adeno-associated virus 9 (AAV9) where shRNA transcription is dependent on Cre recombinase activity, thus restricting shRNA expression to the cardiac ventricle. AAV-shRNAs targeting either Smg1 (AAV9-fl/fl-shSmg1) or Syt17 (AAV9-fl/fl-shSyt17) were administered individually or simultaneously as depicted in Figure XA in the online-only Data Supplement.<sup>31</sup> A scrambled nonsilencing RNA construct was used as control. As shown in Figure XB through XD in the online-only Data Supplement, efficient mRNA and protein knockdown of the respective targets was achieved by

AAV9-mediated shRNA cardiac transduction, whereas *Herna1* RNA levels were maintained (Figure XE in the online-only Data Supplement). Thereafter, mice treated with the respective shRNAs were subjected to sham or TAC surgery. As indicated in Figure XF in the online-only Data Supplement, TAC surgery significantly increased blood flow across the aorta of mice of all groups to a

similar extent. At 4 weeks postsurgery, a dramatic decline in cardiac systolic function was observed in control mice injected with an AAV9 bearing a nonsilencing shRNA (AAV9-fl-fl-nsRNA) and in mice inactivated for *Smg1* in the myocardium. In contrast, mice treated with AAV9-fl/fl-sh*Syt17* revealed normal cardiac function despite TAC-induced pressure overload (Figure XG

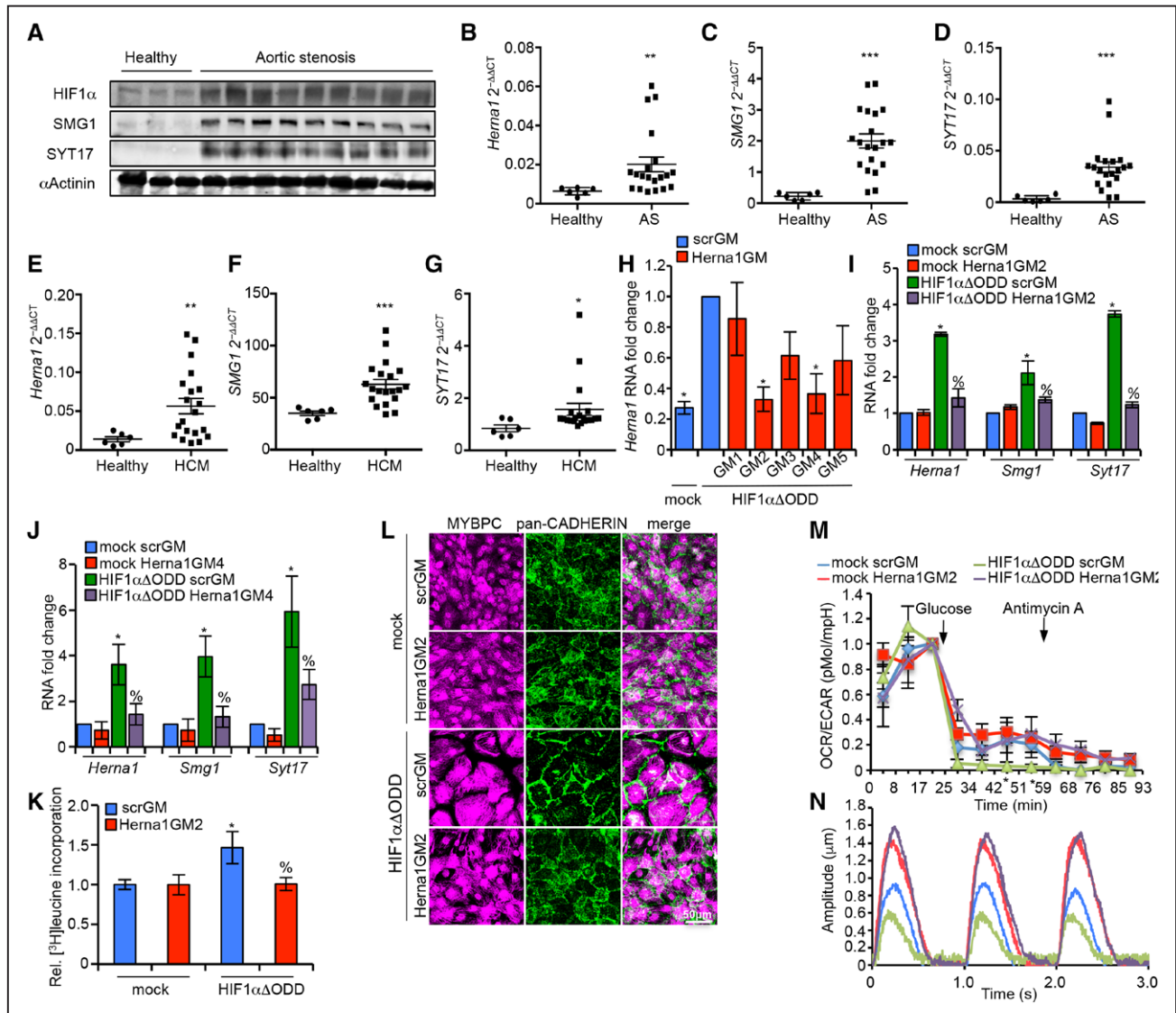


**Figure 8.** Activation of the *HERN1-SMG1-SYT17* axis is relevant in human heart disease and its repression prevents growth and dysfunction in iPSC-hCM.

**A**, Human heart biopsies of healthy subjects and subjects with aortic stenosis were assessed for denoted proteins. Loading is normalized to sarcomeric  $\alpha$ -actinin. **B** through **G**, Human heart biopsies of healthy subjects ( $n=3$ ) and subjects with aortic stenosis (AS,  $n=10$ ; **B** through **D**) or hypertrophic cardiomyopathy (HCM,  $n=10$ ; **E** through **G**) were assessed for denoted RNAs, normalized to *HPRT1* mRNA. Results show duplicated measures. Error bars indicate SE of the mean; \* $P<0.05$  in comparison with healthy control, \*\* $P<0.005$ , \*\*\* $P<0.0005$ ; Mann-Whitney *U* test). **H** through **J**, iPSC-hCM transduced with ectopic HIF1 $\alpha$ ODD or empty vector (mock) were treated with the respective gampers and tested for *Herna1* knockdown (**H** through **J**) or expression of *SMG1* and *SYT17* RNA (**I** and **J**) by qPCR. Values normalized to *HPRT1* mRNA and to cardiomyocytes ectopically expressing HIF1 $\alpha$ ODD and treated with scrGM. **K**, iPSC-hCM transduced as in **I** were assessed for [ $^3$ H]leucine incorporation. **L**, iPSC-hCM treated as in **I** were stained for cardiomyocyte-specific myosin-binding protein C (MYBPC) and pan-cadherin, imaged by confocal microscopy. Representative fields are shown. **M**, iPSC-hCM transduced as in **I** were assessed for oxygen consumption rate (OCR) and extracellular acidification rate (ECAR) after injections of glucose and antimycin A. The OCR to ECAR ratio is shown ( $n=8$  biological replicates for mock scrGM,  $n=9$  for mock Herna1GM2,  $n=10$  for HIF1 $\alpha$ ODD scrGM and HIF1 $\alpha$ ODD Herna1GM2). Error bars indicate SE of the mean. **N**, iPSC-hCM treated as in **I** were stimulated at 1 Hz and assessed for contractile amplitude. Representative traces are shown. **H** through **K**, **N**,  $n=3$  per group. Error bars indicate SD of the mean; **H**, \* $P<0.05$  in comparison with HIF1 $\alpha$ ODD/scrGM-treated iPSC-hCM; 2-way ANOVA with Dunnett post hoc test. **I** through **K**, \* $P<0.05$  in comparison with mock/scrGM-treated iPSC-hCM, % $P<0.05$  in comparison with HIF1 $\alpha$ ODD/scrGM-treated iPSC-hCM; 2-way ANOVA with Tukey post hoc test. **M**, \* $P<0.05$  in comparison with mock/scrGM-treated iPSC-hCM; 2-way ANOVA for repeated measures with Dunnett post hoc test. HIF1 $\alpha$  hypoxia-inducible factor 1 $\alpha$ ; HIF1 $\alpha$ ODD, HIF1 $\alpha$  lacking the oxygen-dependent degradation domain; iPSC-hCM, induced pluripotent stem cell-derived human cardiomyocytes; and qPCR, quantitative polymerase chain reaction.

in the online-only Data Supplement). In accord, lysates of left ventricular biopsies from these mice showed normalized Serca2 protein levels, and increased Ser16-phosphorylation of Phospholamban in comparison with sham or TAC-operated mice injected with AAV9-fl-fl-nsRNA, as well (Figure XD in the online-only Data Supplement). Left ventricular posterior wall thickness was largely normalized by simultaneous inactivation of *Smg1* and *Syt17* (Figure XH in the online-only Data Supplement). In line with these results, cardiac hypertrophy was reduced in TAC-operated mice inactivated for *Smg1* and *Syt17* in the myocardium in comparison with TAC-operated mice treated with AAV9-fl-fl-nsRNA (Figure XI and XJ in the online-only Data Supplement). Thus, simultaneous inactivation of the flanking genes led to normalization of all aspects of cardiac function, dimension, and morphology, hence recapitulating *Herna1* in vivo inactivation.

### Herna1 Correlates With Human Cardiac Hypertrophy and Is Necessary for Disease Transition

In silico analysis indicated conservation of this gene cluster structure in various species, including humans, where *HERNA1* is similarly flanked by *SMG1* and *SYT17* in the genome and shares 38% overall sequence similarity with the mouse homolog (Figure 1B and Figure IIIA and IIIB in the online-only Data Supplement). Hence, we interrogated *HERNA1* function in human cardiomyopathic samples. *HERNA1* induction occurred concomitant to elevated *SMG1* and *SYT17* expression in independent patient cohorts of aortic stenosis-induced cardiomyopathy and idiopathic hypertrophic obstructive cardiomyopathy<sup>31</sup> (Figure 8A through 8G and Table I in the online-only Data Supplement). In contrast, we detected an inverse correlation of the *HERNA1*-*SMG1*-*SYT17* axis in ventricular biopsies of patients with dilative cardiomyopathy and in ventricular biopsies of a Muscle LIM protein (*Mlp*)<sup>-/-</sup> with dilative cardiomyopathy mouse model<sup>32</sup> (Figure XIA through XID in the online-only Data Supplement) likely pointing to an etiology-specific basis for *HERNA1* function.

To determine causality between *HERNA1* transcription and *Smg1* and *Syt17* expression, we identified gapmers targeting *HERNA1* for knockdown in induced pluripotent stem cell-derived human cardiomyocytes (iPSC-hCM). Screening for gapmers targeting human *HERNA1* in iPSC-hCM ectopically expressing HIF1 $\alpha$  $\Delta$ ODD<sup>33</sup> identified gapmers 2 and 4 as effective tools to suppress *HERNA1* production (Figure 8H). Delivery of *HERNA1*GM2 in iPSC-hCM suppressed *HERNA1* expression and attenuated *SMG1* and *SYT17* induction, with similar results observed using *HERNA1*GM4 (Figure 8I and 8J). To assess its impact on pathological

hypertrophy, we depleted *HERNA1* in iPSC-hCM expressing ectopic HIF1 $\alpha$  $\Delta$ ODD and quantified leucine incorporation and 2-dimensional cell size as readouts for cell growth. It is notable that *HERNA1*GM2 inhibited cardiomyocyte hypertrophy (Figure 8K and 8L and Figure XIIA in the online-only Data Supplement). Next, we assayed *HERNA1* function in HIF-driven metabolic reprogramming and cardiomyocyte contractility. As shown in Figure 8M and 8N and Figure XIIB through XIIF in the online-only Data Supplement, *HERNA1*GM2 suppressed the pathological shift to glycolysis and contractile dysfunction caused by HIF1 $\alpha$  $\Delta$ ODD expression. The data obtained from left ventricular biopsies of patients who had pressure-overload heart failure recapitulates the expression profile of the mouse models of left ventricular pressure overload, indicating a potential role for the *HERNA1*-*SMG1*-*SYT17* axis in driving human heart disease. It is more important that the clearly beneficial effects of *HERNA1* depletion in iPSC-hCM protecting from structural, metabolic, and functional remodeling suggests *HERNA1* as a novel RNA target for the treatment of heart failure.

### DISCUSSION

Collectively, this work reports a novel mode of hypoxia-dependent gene regulation in pressure overload-induced heart disease initiated by HIF1 $\alpha$  activation of the *HERNA1* eRNA and its binding to and stimulation of mRNA synthesis of its neighboring gene promoters *SYT17* and *SMG1*. This mode of gene regulation (as opposed to direct transcriptional activation of *SYT17* and *SMG1* by HIF1 $\alpha$ ) provides an effective means of engendering cell-specific hypoxia transcriptional responses and offers a potential mechanistic explanation of at least some of the contextual effects that HIF1 $\alpha$  mediates in different tissues and pathological settings.<sup>34–37</sup> A schematic of this model is shown in Figure XIII in the online-only Data Supplement.

Hence, the requirement for HIF $\alpha$  in development and disease may reflect the need for extensive remodeling of the RNA landscape in cardiac pathology that is known to be coupled to the appearance of transcripts and splice variants of metabolic and sarcomeric proteins not typically expressed in the normal heart.<sup>38–41</sup> In this regard, we have recently uncovered SF3B1-mediated alternative pre-mRNA splicing as a previously unknown step between HIF-driven transcription and metabolism, cell growth, and the development of hypertrophic heart disease.<sup>31</sup> It is conceivable that the activation of both the HIF1 $\alpha$ -SF3B1 and HIF1 $\alpha$ -*HERNA1* axes in response to hypoxia provides a means to coordinately control central posttranscriptional gene regulatory processes to bring about key changes in the RNA landscape essential for implementing adaptive and maladaptive changes in

cell phenotype. Of note, the presented specificity for HIF1 $\alpha$  as a driver of the characterized pathological stress-induced hypoxic response was ensured by the chosen screening strategy, focusing on in vitro and in vivo models where transcript expression was studied as a function of HIF1 $\alpha$  (Figure 1G and 1H and Figures IA, IIB, IIC, and IVA in the online-only Data Supplement).

Given the correlation between *HERNA1*, *SMG1*, and *SYT17* coexpression in independent human cohorts of hypertrophic cardiomyopathy and aortic stenosis, it is conceivable to suggest a role of this axis in driving cardiac pathology. Indeed, suppression of stress-induced *Herna1* production in vivo in mice resolved established cardiomyopathy through repression of *Syt17* and *Smg1* transcription, indicating that a tight coupling of enhancer transcription and successive induction of promoters in their vicinity is disease relevant. Both aortic stenosis (as the most prevalent valvular heart disease) and hypertrophic cardiomyopathy (as the primary cause of sudden cardiac death) represent a large fraction of cardiac disease whose therapy today is inefficient in preventing heart failure. In contrast to the general rather poor sequence conservation of long-noncoding RNAs among mammals, *HERNA1* sequence shares a stretch of 330 bp that displays high sequence conservation among mammals (Figure 1B and Figure IIIA and IIB in the online-only Data Supplement), thus offering a high translational potential through the definition of target sequences that work across species for therapeutic development. In contrast to the nontargeted nature of current treatment regimens, the contextual nature of *HERNA1* expression facilitates specific targeting of the diseased ventricular myocardium. Hence, targeting of context-specific disease-induced eRNAs, such as *HERNA1*, represents an attractive avenue for developing targeted therapeutic modalities for the treatment of a variety of pathologies including heart disease, cancer, diabetes mellitus, and neuropathies.

## ARTICLE INFORMATION

Received July 5, 2018; accepted March 8, 2019.

The online-only Data Supplement is available with this article at <https://www.ahajournals.org/doi/suppl/10.1161/CIRCULATIONAHA.118.036769>.

## Correspondence

Jaya Krishnan, PhD, Institute of Cardiovascular Regeneration, Centre for Molecular Medicine, Goethe-University Frankfurt, Theodor-Stern-Kai 7, 60590 Frankfurt, Germany. Email [Krishnan@med.uni-frankfurt.de](mailto:Krishnan@med.uni-frankfurt.de)

## Affiliations

Institute of Molecular Health Sciences, ETH Zurich, Switzerland (P.M., G.R., N.F., S.T., W.K.). Institute of Clinical Chemistry and Laboratory Medicine, University Hospital Dresden, Germany (P.M., E.H.). MRC Clinical Sciences Centre, Imperial College London, United Kingdom (C.B., S.K., J.K.). Institute of Cardiovascular Regeneration, Centre for Molecular Medicine, Goethe-University Frankfurt, Germany (C.B., M.-D.P., R.S., P.G., S.D., J.K.). Department of Internal Medicine III: Cardiology and Angiology, University of Kiel, Germany (S.S.). Klinik für Kardiologie und Pneumologie, Georg-August-Universität Göttingen and DZHK

(German Centre for Cardiovascular Research) (S.S.). Cardiovascular Assessment Facility, University of Lausanne and CHUV, Switzerland (C.B., A.S.). Department of Anesthesiology and Intensive Care Medicine, University Hospital Schleswig-Holstein, and Department of Anesthesiology and Intensive Care Medicine, University Hospital Leipzig, Germany (S.N.S.). Department of Medicine, University of Lausanne Medical School, Switzerland (T.P.). The current address for Dr Sossalla is Department of Internal Medicine II, University Hospital of Regensburg, Germany, and Klinik für Kardiologie und Pneumologie, Georg-August-Universität Göttingen and DZHK (German Centre for Cardiovascular Research), Germany.

## Acknowledgments

We thank P. Schuster, K. Bottermann, T. Yuan, M. Hammer, S. Gonzalez-Gonggria, N. Xinsheng, J. Eekels, F. Dholoo, and S. Kahn for discussions, help, and technical assistance. We thank E. Ehler, D. Withers, M. Latreille, E. Perriard, and J.C. Perriard for support. Drs Krishnan and Krek designed and Drs Mirtschink, Bischof, Pham, Rossi, and Hagag executed most experiments. Dr Traub performed in vitro contractility analyses and targeted chromatin immunoprecipitation. Dr Bischof and Sarre performed surgeries, echocardiography, and necropsy analysis under the supervision of Dr Pedrazzini. Drs Sharma, Khadayate, and Fankhauser analyzed expression and sequencing data. Drs Sossalla and Stehr provided human biopsies. Drs Rossi and Dimmeler provided constructs and scientific advice. Drs Krishnan, Mirtschink, and Krek, with help from Dr Berthonneche, wrote the article.

## Sources of Funding

This work was supported by grants from the Medical Research Council (MRC: MC1102/4), LOEWE-CGT (21000830) the European Union (GA: 822455) to Dr Krishnan; the Swiss Heart Foundation and Swiss National Sciences Foundation to Dr Krek; the Foundation for Pathobiochemistry and Molecular Diagnostics to Dr Mirtschink; the German Research Foundation (DFG; Exc147 and Exc2026) and the European Research Council (Angiolinc) to Dr Dimmeler; and the German Research Foundation (DFG; Exc147-2 and GR4745/1-1) to Dr Grote.

## Disclosures

None.

## REFERENCES

- Ambrosy AP, Fonarow GC, Butler J, Chioncel O, Greene SJ, Vaduganathan M, Nodari S, Lam CSP, Sato N, Shah AN, Gheorghiadu M. The global health and economic burden of hospitalizations for heart failure: lessons learned from hospitalized heart failure registries. *J Am Coll Cardiol*. 2014;63:1123–1133. doi: 10.1016/j.jacc.2013.11.053
- Ounzain S, Micheletti R, Beckmann T, Schroen B, Alexanian M, Pezzuto I, Crippa S, Nemir M, Sarre A, Johnson R, Dauvillier J, Burdet F, Ibberson M, Guigó R, Xenarios I, Heymans S, Pedrazzini T. Genome-wide profiling of the cardiac transcriptome after myocardial infarction identifies novel heart-specific long non-coding RNAs. *Eur Heart J*. 2015;36:353–68a. doi: 10.1093/eurheartj/ehu180
- Kim TK, Hemberg M, Gray JM, Costa AM, Bear DM, Wu J, Harmin DA, Laptewicz M, Barbara-Haley K, Kuersten S, Markenscoff-Papadimitriou E, Kuhl D, Bito H, Worley PF, Kreiman G, Greenberg ME. Widespread transcription at neuronal activity-regulated enhancers. *Nature*. 2010;465:182–187. doi: 10.1038/nature09033
- Ørom UA, Derrien T, Beringer M, Gumireddy K, Gardini A, Bussotti G, Lai F, Zytnicki M, Notredame C, Huang Q, Guigo R, Shiekhattar R. Long noncoding RNAs with enhancer-like function in human cells. *Cell*. 2010;143:46–58. doi: 10.1016/j.cell.2010.09.001
- Bulger M, Groudine M. Looping versus linking: toward a model for long-distance gene activation. *Genes Dev*. 1999;13:2465–2477.
- Berman BP, Nibu Y, Pfeiffer BD, Tomancak P, Celniker SE, Levine M, Rubin GM, Eisen MB. Exploiting transcription factor binding site clustering to identify cis-regulatory modules involved in pattern formation in the *Drosophila* genome. *Proc Natl Acad Sci USA*. 2002;99:757–762. doi: 10.1073/pnas.231608898
- ENCODE Project Consortium. An integrated encyclopedia of DNA elements in the human genome. *Nature*. 2012;489:57–74. doi: 10.1038/nature11247
- Heintzman ND, Stuart RK, Hon G, Fu Y, Ching CW, Hawkins RD, Barrera LO, Van Calcar S, Qu C, Ching KA, Wang W, Weng Z, Green RD,

- Crawford GE, Ren B. Distinct and predictive chromatin signatures of transcriptional promoters and enhancers in the human genome. *Nat Genet*. 2007;39:311–318. doi: 10.1038/ng1966
9. Lam MT, Cho H, Lesch HP, Gosselin D, Heinz S, Tanaka-Oishi Y, Benner C, Kaikkonen MU, Kim AS, Kosaka M, Lee CY, Watt A, Grossman TR, Rosenfeld MG, Evans RM, Glass CK. Rev-Erbs repress macrophage gene expression by inhibiting enhancer-directed transcription. *Nature*. 2013;498:511–515. doi: 10.1038/nature12209
  10. Li W, Notani D, Ma Q, Tanasa B, Nunez E, Chen AY, Merkurjev D, Zhang J, Ohgi K, Song X, Oh S, Kim HS, Glass CK, Rosenfeld MG. Functional roles of enhancer RNAs for oestrogen-dependent transcriptional activation. *Nature*. 2013;498:516–520. doi: 10.1038/nature12210
  11. De Santa F, Barozzi I, Miettton F, Ghisletti S, Polletti S, Tusi BK, Muller H, Ragoussis J, Wei CL, Natoli G. A large fraction of extragenic RNA pol II transcription sites overlap enhancers. *PLoS Biol*. 2010;8:e1000384. doi: 10.1371/journal.pbio.1000384
  12. Ounzain S, Pezzuto I, Micheletti R, Burdet F, Sheta R, Nemir M, Gonzales C, Sarre A, Alexanian M, Blow MJ, May D, Johnson R, Dauvillier J, Pennacchio LA, Pedrazzini T. Functional importance of cardiac enhancer-associated noncoding RNAs in heart development and disease. *J Mol Cell Cardiol*. 2014;76:55–70. doi: 10.1016/j.yjmcc.2014.08.009
  13. Wang GL, Jiang BH, Rue EA, Semenza GL. Hypoxia-inducible factor 1 is a basic-helix-loop-helix-PAS heterodimer regulated by cellular O<sub>2</sub> tension. *Proc Natl Acad Sci USA*. 1995;92:5510–5514. doi: 10.1073/pnas.92.12.5510
  14. Semenza GL. Hypoxia-inducible factors in physiology and medicine. *Cell*. 2012;148:399–408. doi: 10.1016/j.cell.2012.01.021
  15. Barrick CJ, Rojas M, Schoonhoven R, Smyth SS, Threadgill DW. Cardiac response to pressure overload in 129S1/SvImJ and C57BL/6J mice: temporal- and background-dependent development of concentric left ventricular hypertrophy. *Am J Physiol Heart Circ Physiol*. 2007;292:H2119–H2130. doi: 10.1152/ajpheart.00816.2006
  16. Krishnan J, Suter M, Windak R, Krebs T, Felley A, Montessuit C, Tokarska-Schlattner M, Aasum E, Bogdanova A, Perriard E, Perriard JC, Larsen T, Pedrazzini T, Krek W. Activation of a HIF1 $\alpha$ -PPAR $\gamma$  axis underlies the integration of glycolytic and lipid anabolic pathways in pathologic cardiac hypertrophy. *Cell Metab*. 2009;9:512–524. doi: 10.1016/j.cmet.2009.05.005
  17. Lei L, Mason S, Liu D, Huang Y, Marks C, Hickey R, Jovin IS, Pypaert M, Johnson RS, Giordano FJ. Hypoxia-inducible factor-dependent degeneration, failure, and malignant transformation of the heart in the absence of the von Hippel-Lindau protein. *Mol Cell Biol*. 2008;28:3790–3803. doi: 10.1128/MCB.01580-07
  18. Melo CA, Drost J, Wijchers PJ, van de Werken H, de Wit E, Oude Vrielink JA, Elkon R, Melo SA, L veill  N, Kalluri R, de Laat W, Agami R. eRNAs are required for p53-dependent enhancer activity and gene transcription. *Mol Cell*. 2013;49:524–535. doi: 10.1016/j.molcel.2012.11.021
  19. Stamatoyannopoulos JA, Snyder M, Hardison R, Ren B, Gingeras T, Gilbert DM, Groudine M, Bender M, Kaul R, Canfield T, Giste E, Johnson A, Zhang M, Balasundaram G, Byron R, Roach V, Sabo PJ, Sandstrom R, Stehling AS, Thurman RE, Weissman SM, Cayting P, Hariharan M, Lian J, Cheng Y, Landt SG, Ma Z, Wold BJ, Dekker J, Crawford GE, Keller CA, Wu W, Morrissey C, Kumar SA, Mishra T, Jain D, Byrnska-Bishop M, Blankenberg D, Lajoie BR, Jain G, Sanyal A, Chen KB, Denas O, Taylor J, Blobel GA, Weiss MJ, Pimkin M, Deng W, Marinov GK, Williams BA, Fisher-Aylor KI, Desalvo G, Kiralusha A, Trout D, Amrhein H, Mortazavi A, Edsall L, McCleary D, Kuan S, Shen Y, Yue F, Ye Z, Davis CA, Zaleski C, Jha S, Xue C, Dobin A, Lin W, Fastuca M, Wang H, Guigo R, Djebali S, Lagarde J, Ryba T, Sasaki T, Malladi VS, Cline MS, Kirkup VM, Learned K, Rosenbloom KR, Kent WJ, Feingold EA, Good PJ, Pazin M, Lowdon RF, Adams LB; Mouse ENCODE Consortium. An encyclopedia of mouse DNA elements (Mouse ENCODE). *Genome Biol*. 2012;13:418. doi: 10.1186/gb-2012-13-8-418
  20. Blow MJ, McCulley DJ, Li Z, Zhang T, Akiyama JA, Holt A, Plajzer-Frick I, Shoukry M, Wright C, Chen F, Afzal V, Bristow J, Ren B, Black BL, Rubin EM, Visel A, Pennacchio LA. ChIP-Seq identification of weakly conserved heart enhancers. *Nat Genet*. 2010;42:806–810. doi: 10.1038/ng.650
  21. Baron-Benamou J, Gehring NH, Kulozik AE, Hentze MW. Using the lambdaN peptide to tether proteins to RNAs. *Methods Mol Biol*. 2004;257:135–154. doi: 10.1385/1-59259-750-5:135
  22. Pagel JI, Deindl E. Early growth response 1—a transcription factor in the crossfire of signal transduction cascades. *Indian J Biochem Biophys*. 2011;48:226–235.
  23. Chu C, Qu K, Zhong FL, Artandi SE, Chang HY. Genomic maps of long noncoding RNA occupancy reveal principles of RNA-chromatin interactions. *Mol Cell*. 2011;44:667–678. doi: 10.1016/j.molcel.2011.08.027
  24. Graven KK, Troxler RF, Kornfeld H, Panchenko MV, Farber HW. Regulation of endothelial cell glyceraldehyde-3-phosphate dehydrogenase expression by hypoxia. *J Biol Chem*. 1994;269:24446–24453.
  25. Choudhry H, Albukhari A, Morotti M, Haider S, Moralli D, Smythies J, Sch del J, Green CM, Camps C, Buffa F, Ratcliffe P, Ragoussis J, Harris AL, Mole DR. Tumor hypoxia induces nuclear paraspeckle formation through HIF-2 $\alpha$  dependent transcriptional activation of NEAT1 leading to cancer cell survival. *Oncogene*. 2015;34:4482–4490. doi: 10.1038/onc.2014.378
  26. Shlyueva D, Stampfel G, Stark A. Transcriptional enhancers: from properties to genome-wide predictions. *Nat Rev Genet*. 2014;15:272–286. doi: 10.1038/nrg3682
  27. Wan WB, Migawa MT, Vasquez G, Murray HM, Nichols JG, Gaus H, Berdeja A, Lee S, Hart CE, Lima WF, Swayze EE, Seth PP. Synthesis, biophysical properties and biological activity of second generation antisense oligonucleotides containing chiral phosphorothioate linkages. *Nucleic Acids Res*. 2014;42:13456–13468. doi: 10.1093/nar/gku1115
  28. Lu M, Liu YH, Goh HS, Wang JJ, Yong QC, Wang R, Bian JS. Hydrogen sulfide inhibits plasma renin activity. *J Am Soc Nephrol*. 2010;21:993–1002. doi: 10.1681/ASN.2009090949
  29. Wiesel P, Mazzolai L, Nussberger J, Pedrazzini T. Two-kidney, one clip and one-kidney, one clip hypertension in mice. *Hypertension*. 1997;29:1025–1030.
  30. Chen J, Kubalak SW, Chien KR. Ventricular muscle-restricted targeting of the RXR $\alpha$  gene reveals a non-cell-autonomous requirement in cardiac chamber morphogenesis. *Development*. 1998;125:1943–1949.
  31. Mirtschink P, Krishnan J, Grimm F, Sarre A, H rl M, Kayikci M, Fankhauser N, Christinat Y, Cortijo C, Feehan O, Vukolic A, Sossalla S, Stehr SN, Ule J, Zamboni N, Pedrazzini T, Krek W. HIF-driven SF3B1 induces KHK-C to enforce fructolysis and heart disease. *Nature*. 2015;522:444–449. doi: 10.1038/nature14508
  32. Arber S, Hunter JJ, Ross J Jr, Hongo M, Sansig G, Borg J, Perriard JC, Chien KR, Caroni P. MLP-deficient mice exhibit a disruption of cardiac cytoarchitectural organization, dilated cardiomyopathy, and heart failure. *Cell*. 1997;88:393–403.
  33. Huang LE, Gu J, Schau M, Bunn HF. Regulation of hypoxia-inducible factor 1 $\alpha$  is mediated by an O<sub>2</sub>-dependent degradation domain via the ubiquitin-proteasome pathway. *Proc Natl Acad Sci USA*. 1998;95:7987–7992. doi: 10.1073/pnas.95.14.7987
  34. Vanharanta S, Shu W, Brenet F, Hakimi AA, Heguy A, Viale A, Reuter VE, Hsieh JJ, Scandura JM, Massagu  J. Epigenetic expansion of VHL-HIF signal output drives multiorgan metastasis in renal cancer. *Nat Med*. 2013;19:50–56. doi: 10.1038/nm.3029
  35. Lu X, Yan CH, Yuan M, Wei Y, Hu G, Kang Y. *In vivo* dynamics and distinct functions of hypoxia in primary tumor growth and organotropic metastasis of breast cancer. *Cancer Res*. 2010;70:3905–3914. doi: 10.1158/0008-5472.CAN-09-3739
  36. Choudhry H, Sch del J, Oikonomopoulos S, Camps C, Grampp S, Harris AL, Ratcliffe PJ, Ragoussis J, Mole DR. Extensive regulation of the non-coding transcriptome by hypoxia: role of HIF in releasing paused RNApol2. *EMBO Rep*. 2014;15:70–76. doi: 10.1002/embr.201337642
  37. Hsu T. Complex cellular functions of the von Hippel-Lindau tumor suppressor gene: insights from model organisms. *Oncogene*. 2012;31:2247–2257. doi: 10.1038/onc.2011.442
  38. Kong SW, Hu YW, Ho JW, Ikeda S, Polster S, John R, Hall JL, Bisping E, Pieske B, dos Remedios CG, Pu WT. Heart failure-associated changes in RNA splicing of sarcomere genes. *Circ Cardiovasc Genet*. 2010;3:138–146. doi: 10.1161/CIRCGENETICS.109.904698
  39. Lara-Pezzi E, G mez-Salinerio J, Gatto A, Garc a-Pav a P. The alternative heart: impact of alternative splicing in heart disease. *J Cardiovasc Transl Res*. 2013;6:945–955. doi: 10.1007/s12265-013-9482-z
  40. Wharton J, Morgan K, Rutherford RA, Catravas JD, Chester A, Whitehead BF, De Leval MR, Yacoub MH, Polak JM. Differential distribution of angiotensin AT<sub>2</sub> receptors in the normal and failing human heart. *J Pharmacol Exp Ther*. 1998;284:323–336.
  41. Agarkova I, Auerbach D, Ehler E, Perriard JC. A novel marker for vertebrate embryonic heart, the EH-yomesin isoform. *J Biol Chem*. 2000;275:10256–10264. doi: 10.1074/jbc.275.14.10256